Pixel-Based Rust Severity Classification on Steel Surfaces Using HSI Features and Machine Learning Techniques

Shahinuzzaman[1], Po-Han Chen[2] , Emadaldeen Benshaaban[3]

[1,2,3] Department of Building, Civil and Environmental Engineering, Concordia University, Montreal, QC, Canada
s_sujon@live.concordia.ca, pohan.chen@concordia.ca, emadaldeen.benshaaban@concordia.ca

Abstract

Ensuring the safety and longevity of steel structures, like bridges and buildings, depends on the effective monitoring of rust and its severity. Traditional methods of rust detection often rely on visual inspections, which can be subjective and time-consuming. In this paper, we present a more efficient way to classify rust severity on steel surfaces using the HSI color space, along with pixel value analysis and computer vision techniques. By utilizing the different components of the HSI color model, we improve the accuracy of rust segmentation, which helps in better identifying the severity levels of rust. This method analyzes individual pixel values in images of steel surfaces, providing a detailed understanding of the rust's extent and intensity. Additionally, we conducted histogram analysis to calculate the mean and standard deviation of pixel values for assessing rust severity. Our machine learning framework, which includes Random Forest and OpenCV, processes high-resolution images to classify rust severity automatically through image segmentation and thresholding techniques. This method also incorporates the K-means algorithm with the Elbow Method to determine the optimal number of clusters and perform segmentation automatically. The results show that this approach offers a more precise and objective way of assessing rust damage according to the severity compared to traditional inspection methods.

Keywords –

Rust segmentation, Rust severity identification, steel surface, HIS color space, Pixel value analysis

1 Introduction

Rust on the steel surfaces of civil engineering structures is a prevalent problem that may pose significant safety hazards. [1], [2], [3]. The corrosion of steel structures poses a considerable challenge for engineers globally. [4], and prompt and precise monitoring of rust damage on steel surfaces is crucial to maintaining the structural integrity, safety, and durability of steel facilities [5],[6]. Conventional rust examination on steel surfaces, particularly for bridges, is laborious, time-consuming, and occasionally hazardous [6] . Since the late 1990s, vision-based image processing techniques have garnered significant attention for inspecting surface defects in infrastructure, such as rust and cracks [7], [8], [9], [10]. Corrosion, including rust, costs the global economy an estimated $2.5 trillion, equivalent to 3.4% of global GDP. Proper monitoring and preventive measures could reduce this cost by up to 35%, potentially saving US$875 billion [11]. In high-risk industries like construction, rust-induced structural failures are a significant cause of accidents. In 2022, for example, 1,056 fatalities occurred in the construction sector, with 423 deaths resulting from falls, slips, or trips [12].

Computer vision involves methodologies that allow machines to interpret the visual environment via digital photographs via machine learning algorithms. Visual media, including images and videos, are the predominant inputs for computer vision applications [13]. Computer vision-based structural health monitoring (CV-SHM) has garnered considerable interest in infrastructure management, including crack, rust, etc. Many computer vision techniques are available for surface defect detection, such as crack, which focus on the analysis of linear features and structural discontinuities, often using geometric modeling techniques. However, these techniques are less effective for rust detection, where the primary focus is on color variation, texture analysis, and corrosion patterns specific to rust. This methodology includes several techniques, including image classification, object detection, object segmentation, visual tracking, 3D reconstruction, image generation, image enhancement, pose estimation, action recognition, image captioning and optical flow analysis [14], [15]. The most common techniques are classification, detection, and segmentation. Segmentation is divided into two types: semantic segmentation and instance segmentation. Semantic segmentation labels every pixel of an object but doesn't distinguish between individual items in the same group. On the other hand, instance segmentation not only labels the pixels but also identifies and separates each instance of the same object (Figure 1) [16]. Computer Vision (CV) techniques are sophisticated instruments for assessing structural integrity, facilitating non-contact monitoring with great precision [17]. When combined with deep learning, computer vision markedly improves object detection abilities[17], [18].

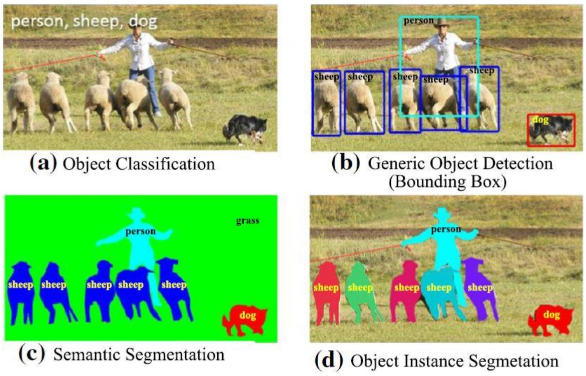

Figure 1. Computer vision techniques: a) image-level object classification, b) bounding box level generic object detection, c) pixel-wise semantic segmentation, d) instance-level semantic Segmentation [19].

2 Related work

We have organized our literature review into two main areas: (1) color space and (2) pixel value analysis

2.1 Color Space

Color properties are a fundamental part of image analysis because they help us understand the visual details in an image, such as pixel values and textures. Different color spaces, like RGB, HSI, and LAB, YCbCr each have their unique ways of representing color, using different shapes and ranges of pixel values. [20], [21]. The most commonly used color space is the three-channel Red, Green, and Blue (RGB) color space (Figure 2.) . In the RGB color space, each channel (Red, Green, and Blue) can represent 256 different values, ranging from 0 to 255, in an 8-bit image. This means that for each color channel, there are 256 possible intensity levels. For example, when the pixel values are (0, 0, 0), it represents pure black, with no color present. On the other hand, when the pixel values are (255, 0, 0), it indicates the maximum intensity of red. With 256 possible values for each of the three channels, the total number of possible colors in the RGB color space is 256 x 256 x 256, or about 16 million different colors.[20].

The conversion of images from RGB to grayscale is a common technique in image processing, as well as in rust identification. [2]. In 1995, FURUTAI et al. [22] Proposed a model for structural damage assessment caused by corrosion using the hue, saturation, and value (HSV) color space. This approach was first applied to color space with image processing. Bridge paint assessment through image processing proposed by Chen and Chang in 2003 [23]. The authors transformed all RGB photos into grayscale and delineated three regions according to the illumination conditions of the rust images. In 2004, Choi and Kim [24] employed the Hue (H), Saturation (S), and Intensity (I) HSI color space for corrosion detection and the identification of five unique corrosion types. In 2006, Lee et al. [25] proposed the utilization of color image rather than grayscale images to inspect steel bridge surface coatings. One of the initial methodologies in color space analysis for image processing was introduced by Chen et al. [26]. The authors examined 14 color spaces to identify the most effective one for addressing non-illumination issues. Similarly, Shen et al. [8] Investigated 19 color spaces, including grayscale, to address non-illumination problems in images.

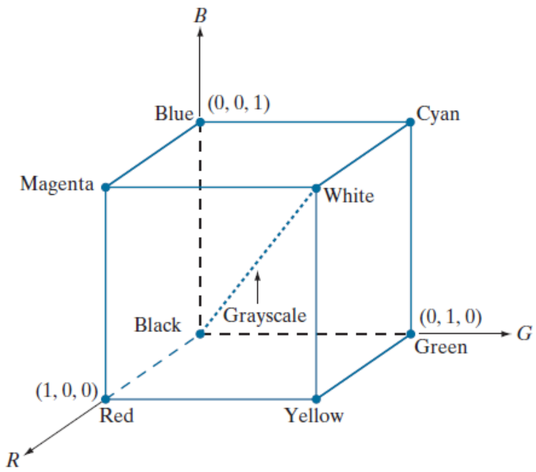

Figure 2. RGB three-dimensional Color cube [26].

Kuo-Wei Liao et al. [27] suggested an automated method for rust identification on a steel bridge utilizing digital image analysis. They employed three picture recognition methodologies: (1) K-means clustering in the hue channel, (2) double-center-double-radius (DCDR) method for RGB color space, and (3) DCDR algorithm for Hue-Saturation-Intensity (HSI) color space. The authors compared 12 color spaces (RGB, HIS, YPbPr, YCbCr, JPEG-YCbCr, YDbDr, YIQ, YUV, HSV, XYZ, LAB, CAT02 LMS) and determined that the Hue characteristic was essential and more efficacious. Yundong Li et al. [28] Converted the RGB image into the YCbCr color space and calculated only the Cr component using the Otsu method to identify rust.

2.2 Pixel Value Analysis

Pixel is the most commonly used term to refer to the components of a digital image [20]. In one of the earliest studies on rust identification, Chen et al. (2009) [26] converted RGB images into the Hue, Saturation, and Intensity (HSI) color space to analyze pixel values associated with rust. Their findings revealed that the mean pixel values in the RGB space were (R, G, B) = (173.22, 107.76, 60.54), while in the HSI space, the means were (H, S, I) = (24.4909, 0.4646, 0.4471). The corresponding standard deviations in the HSI space were (H, S, I) = (6.5469, 0.1498, 0.1442). In 2023, Sun et al. [3] analyzed corrosion using pixel scatter diagrams in the RGB color space. They calculated the mean pixel values as C (R, G, B) = (193.94, 123.57, 59.10) and the standard deviations as σ(R, G, B) = (29.88, 29.12, 17.92).

3 Methodology

Our methodology is divided into two segments. The first segment involves calculating the mean and standard deviation of HIS pixel values. The second segment focuses on training and predicting rust severity.

3.1 Statistical Analysis of HIS Pixel Values

3.1.1 Converting Image from RGB to HSI

Pixel values constitute the essential components and smallest units of a digital image [29]. For this study, we collected data from diverse and heterogeneous sources, including mobile phones, digital cameras, drones, and open-source repositories. This diversity ensures that the dataset reflects a wide range of real-world scenarios. Typically, digital cameras and mobile phones produce images in the Red, Green, and Blue (RGB) color model by default. To enhance the utility of the dataset, especially for addressing challenges like shadow removal and effectively identifying rust severity in the images, we converted all collected data from the RGB color space to the Hue, Saturation, and Intensity (HSI) color space. The range of RGB values is typically 0 to 255 for an 8-bit image [20], as discussed in the previous section. For this study, we normalized the RGB values to fit the HSI color model, where the intensity and saturation values are scaled to a range of 0 to 1, and the hue values are normalized to a range of 0 to 360 degrees using the following formula (Equations 1-4).

$$H\ (Hue) = \begin{cases} \theta & if\ B \leq G \\ 360 - \theta & if\ B > G \end{cases} \tag{1}$$

with

$$\theta = Cos^{-1}\left\{\frac{\frac{1}{2}\left[(R-G)+(R-B)\right]}{\left[(R-G)^2+(R-B)(G-B)\right]^{\frac{1}{2}}}\right\} \tag{2}$$

$$S(Sat.) = 1 - \frac{3}{(R+G+B)}\left[\min(R,G,B)\right] \tag{3}$$

$$I\ (Intensity) = \frac{1}{3}\ (\mathrm{R}+\mathrm{G}+\mathrm{B}) \tag{4}$$

Hue represents the type of color Hue represents the type of color (e.g., red, blue, green) and is expressed in degrees (0°–360°). Saturation measures the purity of the color. It is computed as the proportion of the maximum deviation of the pixel color values from the neutral gray level. The intensity is the average of the three RGB components and represents the brightness of the pixel.

3.1.2 Optimal Number of Clusters Using Elbow Method and K-Means Clustering

Unsupervised machine learning, particularly the k-means clustering algorithm, is widely regarded as one of the most popular and efficient techniques for image clustering [30]. Despite its advantages, a significant limitation of k-means is that it requires the number of clusters to be predefined before the clustering process. This can be challenging when dealing with real-world data, where the optimal number of clusters is not known in advance. To resolve this issue, we utilized the Elbow Method, a commonly employed heuristic for identifying the ideal number of clusters. This method entails computing the within the sum of cluster squared (WCSS) distances (inertia) (Equation 5) between each data point and its respective cluster centroid across various cluster characteristics. The results are subsequently displayed to generate an inertia curve. The 'elbow' or 'knee' point of this curve signifies the appropriate number of clusters since it denotes the juncture when the addition of further clusters yields negligible enhancement in diminishing inertia, reflecting a balance between model complexity and efficacy.

To enhance precision and automation, we employed a knee locator algorithm that correctly determines the elbow position in the curve. By integrating k-means with the Elbow Method, we established a rigorous and data-driven strategy to ascertain the appropriate number of clusters, therefore enhancing the efficiency and precision of our picture clustering procedure.

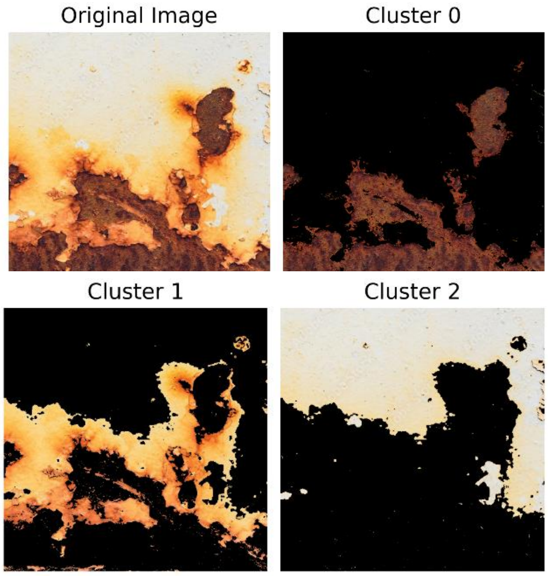

Figure 1. Rust image clustering using the k-means algorithm to visualize and evaluate rust severity in accordance with the AASHTO-2019 standards.

$$\text{Inertia (WCSS)} = \sum_{i=1}^{k} \sum_{x \in C_i} \|x - \mu_i\|^2 \quad (5)$$

- k is the number of clusters
- Ci= The set of points assigned to the cluster i
- x= A data point in cluster Ci
- μ_i= The centroid of cluster Ci

In this paper, we consider three levels of rust severity: Severe, Major, and Minor. These categories were derived from the guidelines provided by the American Association of State Highway and Transportation Officials (AASHTO) in their 'Manual for Bridge Element Inspection 2019' [31]. This guidebook serves as a reliable resource for evaluating bridge conditions, including rust assessment. To comply with these requirements, we assessed rust severity by categorizing photos into separate clusters (Figure 1). Each cluster was subsequently aligned with one of the severity categories established by AASHTO. This methodology enabled us to categorize rust patterns according to picture attributes while maintaining alignment with industry standards. Utilizing these clusters, we can systematically identify and assess the degree of rust.

3.1.3 Histogram Analysis

A histogram is a graphical depiction that illustrates the frequency distribution of a dataset. In image analysis, histograms are frequently employed to examine the distribution of pixel values over various color spaces, including Hue, Saturation, and Intensity (HSI). Due to the absence of publicly available rust specific datasets, we collected a set of 30 real-world images of rusted steel surfaces. These images were analyzed using histogram-based techniques to calculate the mean and standard deviation (SD) of pixel values corresponding to varying rust severity levels. These pixel ranges were then used to train a Random Forest model, aimed at classifying rust severity based on the calculated values.

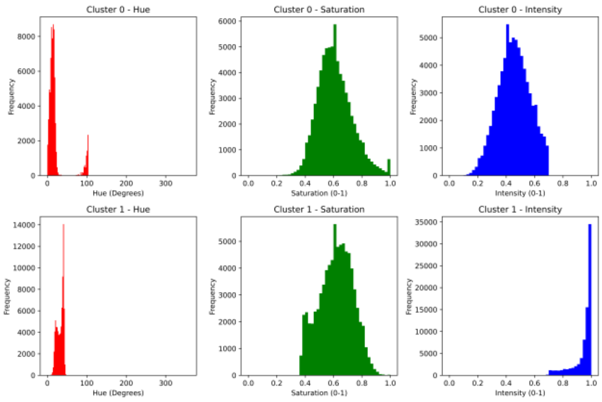

Figure 2. Histograms of H(Hue), S(Saturation), and I (Intensity) for Cluster 0 in HSI Color Space.

From Figure 1, we focused our analysis on Clusters 0 and 1, as Cluster 2 primarily represented the background and did not contain rust. We conducted a histogram analysis to determine the range of pixel values corresponding to different categories of rust severity.

The histograms, as shown in Figure 2, represent the distribution of HSI values for Cluster 0 and Cluster 1. In Cluster 0, the Hue values predominantly range from approximately 0 to 100. The mean Hue value for Cluster-0 is 20.11, with a standard deviation of 26.30. The saturation histogram displays a pyramid-shaped distribution with values ranging between 0.4 and 0.8, indicating a moderate degree of color vibrancy within this cluster. The mean saturation value is 0.61, with a standard deviation of 0.12. Similarly, the intensity histogram follows mid-intensity values of 0.2 to 0.7. The mean intensity value is 0.45, with a standard deviation of 0.11. These histograms provide a detailed overview of the color characteristics and brightness distribution within Cluster 0. A similar analysis was conducted for Cluster 1 further to compare the distinct HSI properties of the clusters.

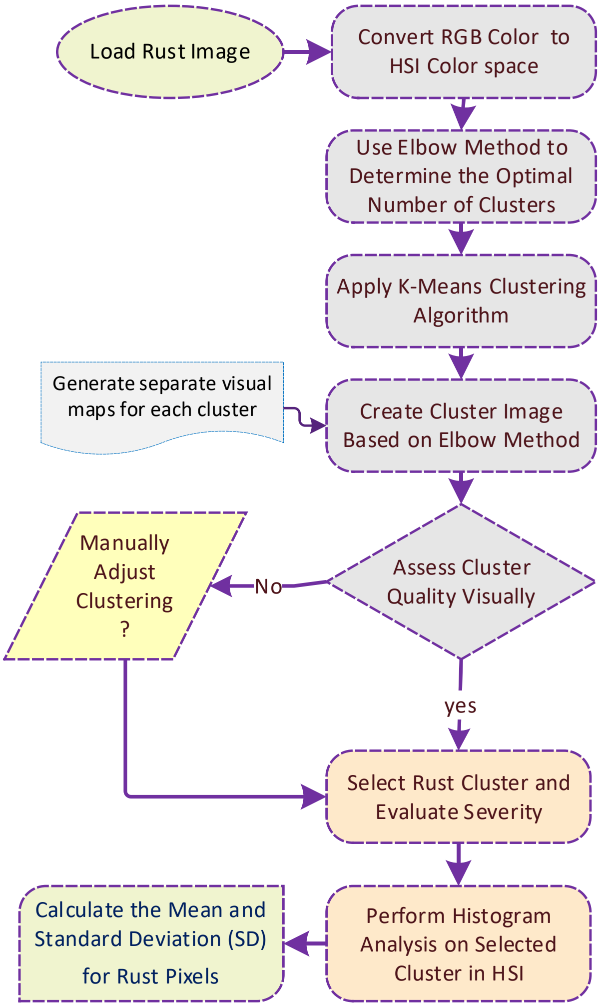

Figure 3. Workflow for Rust Severity Analysis Using Clustering and HSI Histogram Analysis.

We conducted this histogram analysis on 30 rust images and calculated the mean and standard deviation values for rust severity in the HSI color space (Table 1).

Table 1 Mean and Standard Deviation of HSI Pixel Values for Rust Severity Classification.

Severity Pixel	H	SD	S	SD	I	SD
Severe	18.4	16.5	0.65	0.13	0.44	0.14
Major	24.54	12.39	0.61	0.11	0.60	0.09
Minor	47.98	15.80	0.42	0.12	0.68	0.08

The methodology illustrated in Figure 3. provides a systematic process for analyzing rust in images. The process begins by loading the image and converting its colors from RGB to HSI, facilitating a focus on the significant color attributes associated with rust. The Elbow Method is employed to determine the optimal number of groups for segmenting the image, followed by the application of K-means clustering to form these clusters. Visual representations for each cluster are generated and amalgamated into a singular image to validate the coherence of the clustering. If the findings are inaccurate, manual changes might be implemented to enhance the segmentation. Upon accurate identification of the rust regions, the rust cluster is chosen for subsequent study. Analyzing the cluster's color distribution through a histogram and computing essential statistics such as the mean and standard deviation of the rust pixels facilitates the assessment of rust severity in the image. This approach guarantees a comprehensive and accurate analysis.

3.2 Rust Severity Training and Prediction

3.2.1 Training Random Forest Models with Synthetic Data

After calculating the pixel values, we created synthetic data using the mean and standard deviation values derived from our analysis. A Random Forest machine learning algorithm was trained on this synthetic dataset, enabling us to classify rust severity levels. Using the trained model, we generated a set of virtual images based on the input pixel characteristics and applied the trained model to classify external images effectively.

The proposed methodology involves a systematic approach to rust severity classification and segmentation. Synthetic training data is first produced by establishing criteria for hue, saturation, and intensity (HSI) values that align with designated rust severity levels: Severe, Major, and Minor. These criteria are established on the observed mean ± standard deviation values obtained from histogram analysis. A labeled dataset is generated by simulating HSI data points for each severity level based on these thresholds. This dataset is utilized to train a Random Forest classifier, a resilient and adaptable supervised machine learning technique. The dataset is divided into training and testing subsets, and the model's performance is meticulously assessed using metrics including accuracy and F1-score to verify its dependability.

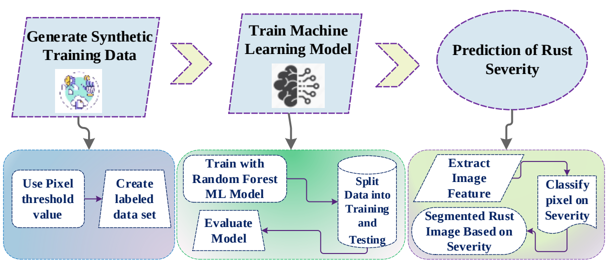

Figure 4. Workflow for Rust Severity Training and Prediction Using Machine Learning Models.

Upon completion of training, the model is utilized on actual photos. Pixel-wise HSI features are derived from the input image by transforming it from RGB to the HSI color space and restructuring the pixel values into a format suitable for the Random Forest model. The trained classifier forecasts the rust severity level Severe, Major, or Minor for each pixel in the image according to its HSI properties. The severity levels are represented by specific colors: Red for Severe, Orange for Major, and Yellow for Minor.

3.2.2 Prediction of Rust Severity

In the concluding phase, the trained Random Forest classifier was utilized to predict the rust severity category for each pixel in the input image, relying on its hue, saturation, and intensity (HSI) attributes. The anticipated labels were assigned numerical values that correspond to established severity levels: Severe, Major, Minor, and Background. The predictions were subsequently reformulated to match the original image dimensions, resulting in a segmentation map. The segmentation outcome, alongside the original image, offered a distinct representation of rust severity levels across the surface (Figure 5). This visual depiction enables accurate identification of rust damage and offers a quantitative framework for evaluating rust severity. This paper incorporates morphological operations techniques to fine-tune the segmented image. A 2×2 kernel was applied for erosion and dilation, refining the boundaries and reducing noise to enhance the segmentation quality.

4 Result

The K-means clustering algorithm was successfully applied, incorporating the elbow method to analyze histogram data. Based on this analysis, the mean and standard deviation of pixel values for each severity level were calculated, as detailed in Table 1. Using the calculated mean and standard deviation values, synthetic data was generated to represent numeric pixel values, which were then used to train a Random Forest machine learning model. The model's performance was evaluated, achieving an F1 score of 0.75, a precision of 0.74, and an accuracy of 0.81. The segmentation outcomes delineated distinct borders among the clusters, offering a visual depiction of rust severity over the surface. A pixel-based analysis was performed to measure the area occupied by each cluster. The image-1 comprised a total of 512*512= 262,144 pixels, with 69775 pixels (26.62%) indicative of Severe rust, 30929 pixels (11.80%) indicative of Major rust, and 52150 pixels (19.89%) indicative of Minor rust.

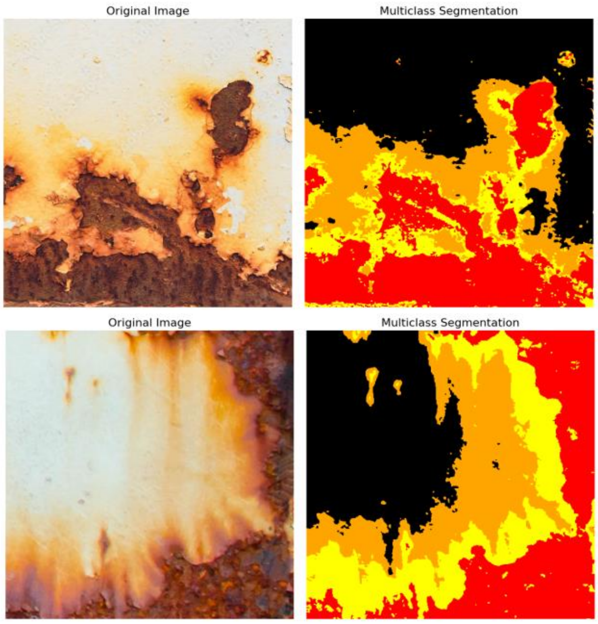

Figure 5. Original and Multiclass Segmentation image of Rust Severity (Severe: Red, Major: Yellow, Minor: Orange, Background: Black).

The Background comprised 109290 pixels (41.69%) of the image area. This quantitative research illustrates the efficacy of the clustering method in detecting and categorizing areas of differing rust intensity, offering significant insights for surface condition evaluation.

5 Discussion

The classification of rust severity is essential for corrosion monitoring and management, especially in industrial settings, where prompt detection can avert structural failures and minimize maintenance expenses. This study utilized an innovative method that integrates clustering-based analysis with machine learning to categorize rust severity into three unique classifications: severe, major, and minor. This workflow integrates unsupervised and supervised methodologies to attain precise and fast segmentation. The conversion of RGB photos to the HSI color space was crucial in the study. In contrast to RGB, the HSI model separates color intensity from chromaticity, offering a more comprehensible depiction of rust attributes under different lighting circumstances. This preprocessing procedure guaranteed that rust segmentation was resilient to shadows and inconsistent lighting, hence improving the dependability of future clustering and classification. The utilization of the Elbow method to ascertain the ideal number of clusters offered an unsupervised approach for segmenting the rusted areas based on pixel similarity. K-means clustering enhanced this segmentation by categorizing pixels into discrete clusters, denoting areas with differing rust intensity. The computed mean and standard deviation (SD) values of pixel HSI components for each cluster facilitated the creation of synthetic data, which constituted the training basis for machine learning models.

A supervised machine learning method, specifically the Random Forest algorithm, was employed to categorize rust severity. This approach was selected for its resilience, capacity to manage high-dimensional data, and interpretability. Through training on synthetic data generated from computed HSI thresholds, the model demonstrated effective generalization to novel images. The evaluation criteria, including accuracy, precision, recall, and F1-score, validated the model's efficacy, with findings affirming its ability to effectively forecast rust severity across various test samples.

6 Conclusion and Future Research

This study significantly contributes by integrating histogram-based analysis with machine learning. The technology integrates traditional image processing with data-driven approaches by utilizing statistical features of pixel distributions, including mean and standard deviation. This hybrid approach guarantees that the classification of rust severity is both comprehensible and scalable for practical applications. Moreover, the visual depiction of segmented output images provides actionable insights, with pixels color-coded by severity. Morphological operations with a 2×2 kernel further refined the segmentation by enhancing boundary accuracy and reducing noise, enabling users to assess the degree and spread of rust intuitively. This quantitative approach provides a dependable decision-making instrument for rust monitoring, facilitating tailored interventions to reduce rust damage successfully.

Notwithstanding its advantages, the proposed methodology does have several limitations. One significant limitation is the reliance on synthetic data specifically, pixel value ranges (mean and standard deviation) derived from a small set of 30 real-world images. Due to the lack of publicly available rust datasets, we used these 30 real-world images to generate the necessary training data. While this approach provides a controlled dataset, the small size and lack of diversity may limit the model's generalization ability, especially with varying rust conditions. Furthermore, external factors like illumination fluctuations and surface texture variations can influence the model's predictions.

Despite these limitations, the approach remains a valuable starting point. Future work will aim to tackle these challenges by expanding the dataset, incorporating a wider variety of real-world images, and integrating adaptive thresholds to account for varying conditions. Additionally, exploring advanced techniques such as deep learning could enhance model generalization and accuracy. This study’s methodology, while in need of further refinement, offers a realistic and scalable solution for classifying rust severity. By combining clustering, machine learning, and quantitative analysis, we establish a solid framework that can be further developed for industrial applications, improving both efficiency and precision in rust severity management systems.

7 Reference

[1] I. Katsamenis, N. Doulamis, A. Doulamis, E. Protopapadakis, and A. Voulodimos, “Simultaneous Precise Localization And Classification of metal rust defects for robotic-driven maintenance and prefabrication using residual attention U-Net,” *Autom Constr*, vol. 137, May 2022, doi: 10.1016/j.autcon.2022.104182.

[2] A. Rahman, ; Zheng, Y. Wu, M. Asce, and R. Kalfarisi, “Semantic Deep Learning Integrated with RGB Feature-Based Rule Optimization for Facility Surface Corrosion Detection and Evaluation,” 2021, doi: 10.1061/(ASCE).

[3] L. Sun, Y. Li, X. Li, and C. Liu, “Corrosion defect segmentation method based on superpixel feature cascade,” *Ain Shams Engineering Journal*, vol. 15, no. 2, Feb. 2024, doi: 10.1016/j.asej.2023.102425.

[4] H. U. Sajid and R. Kiran, “Influence of corrosion and surface roughness on wettability of ASTM A36 steels,” *J Constr Steel Res*, vol. 144, pp. 310–326, May 2018, doi: 10.1016/j.jcsr.2018.01.023.

[5] Y. Zhang, B. M. Ayyub, and J. F. Fung, “Projections of corrosion and deterioration of infrastructure in United States coasts under a changing climate,” *Resilient Cities and Structures*, vol. 1, no. 1, pp. 98–109, Mar. 2022, doi: 10.1016/j.rcns.2022.04.004.

[6] C. Y. Liu and J. S. Chou, “Bayesian-optimized deep learning model to segment deterioration patterns underneath bridge decks photographed by unmanned aerial vehicle,” *Autom Constr*, vol. 146, Feb. 2023, doi: 10.1016/j.autcon.2022.104666.

[7] S. Jiang, Y. Wu, and J. Zhang, “Bridge coating inspection based on two-stage automatic method and collision-tolerant unmanned aerial system,” *Autom Constr*, vol. 146, Feb. 2023, doi: 10.1016/j.autcon.2022.104685.

[8] H. K. Shen, P. H. Chen, and L. M. Chang, “Automated steel bridge coating rust defect

recognition method based on color and texture feature," *Autom Constr*, vol. 31, pp. 338–356, 2013, doi: 10.1016/j.autcon.2012.11.003.

[9] S. Lee, L. M. Chang, and M. Skibniewski, "Automated recognition of surface defects using digital color image processing," *Autom Constr*, vol. 15, no. 4, pp. 540–549, Jul. 2006, doi: 10.1016/j.autcon.2005.08.001.

[10] N. Dhanachandra, K. Manglem, and Y. J. Chanu, "Image Segmentation Using K-means Clustering Algorithm and Subtractive Clustering Algorithm," in *Procedia Computer Science*, Elsevier, 2015, pp. 764–771. doi: 10.1016/j.procs.2015.06.090.

[11] E. Bowman, N. Thompson, D. Gl, O. Moghissi, M. Gould, and J. Payer, "International Measures of Prevention, Application, and Economics of Corrosion Technologies Study," 2016. Accessed: Sep. 30, 2024. [Online]. Available: National Association of Corrosion Engineers (NACE)

[12] Bureau of Labor Statistics, "NATIONAL CENSUS OF FATAL OCCUPATIONAL INJURIES IN 2022," Dec. 2023. [Online]. Available: www.bls.gov/iif

[13] A. A. I. M. Ali *et al.*, "Computer Vision and Image Processing Approaches for Corrosion Detection," Oct. 01, 2023, *Multidisciplinary Digital Publishing Institute (MDPI)*. doi: 10.3390/jmse11101954.

[14] Y. Wang, U. Ahsan, H. Li, and M. Hagen, "A Comprehensive Review of Modern Object Segmentation Approaches," 2022, *Now Publishers Inc*. doi: 10.1561/0600000097.

[15] C. Z. Dong and F. N. Catbas, "A review of computer vision–based structural health monitoring at local and global levels," Mar. 01, 2021, *SAGE Publications Ltd*. doi: 10.1177/1475921720935585.

[16] picsellia.com, "Segmentation vs Detection vs Classification in Computer Vision: A Comparative Analysis." Accessed: Feb. 29, 2024. [Online]. Available: https://www.picsellia.com/post/segmentation-vs-detection-vs-classification-in-computer-vision-a-comparative-analysis

[17] B. Kim, N. Yuvaraj, H. W. Park, K. R. S. Preethaa, R. A. Pandian, and D. E. Lee, "Investigation of steel frame damage based on computer vision and deep learning," *Autom Constr*, vol. 132, Dec. 2021, doi: 10.1016/j.autcon.2021.103941.

[18] Y. J. Cha, K. You, and W. Choi, "Vision-based detection of loosened bolts using the Hough transform and support vector machines," *Autom Constr*, vol. 71, no. Part 2, pp. 181–188, Nov. 2016, doi: 10.1016/j.autcon.2016.06.008.

[19] L. Liu *et al.*, "Deep Learning for Generic Object Detection: A Survey," *Int J Comput Vis*, vol. 128, no. 2, pp. 261–318, Feb. 2020, doi: 10.1007/s11263-019-01247-4.

[20] R. C. . Gonzalez and R. E. . Woods, *Digital image processing*. Pearson, 2018.

[21] F. - Ponce, "Computer Vision - A Modern Approach."

[22] H. Furutai, T. Deguch12, and M. Kushida3, "Neural Network Analysis of Structural Damage Due to Corrosion," Osaka, Japan, Sep. 1995. doi: 10.1109/ISUMA.1995.527678.

[23] P. H. Chen and L. M. Chang, "Artificial intelligence application to bridge painting assessment," *Autom Constr*, vol. 12, no. 4, pp. 431–445, Jul. 2003, doi: 10.1016/S0926-5805(03)00016-5.

[24] K. Y. Choi and S. S. Kim, "Morphological analysis and classification of types of surface corrosion damage by digital image processing," *Corros Sci*, vol. 47, no. 1, pp. 1–15, Jan. 2005, doi: 10.1016/J.CORSCI.2004.05.007.

[25] S. Lee, L. M. Chang, and M. Skibniewski, "Automated recognition of surface defects using digital color image processing," *Autom Constr*, vol. 15, no. 4, pp. 540–549, Jul. 2006, doi: 10.1016/j.autcon.2005.08.001.

[26] P. H. Chen, Y. C. Yang, and L. M. Chang, "Automated bridge coating defect recognition using adaptive ellipse approach," *Autom Constr*, vol. 18, no. 5, pp. 632–643, Aug. 2009, doi: 10.1016/j.autcon.2008.12.007.

[27] K. W. Liao and Y. T. Lee, "Detection of rust defects on steel bridge coatings via digital image recognition," *Autom Constr*, vol. 71, no. Part 2, pp. 294–306, Nov. 2016, doi: 10.1016/j.autcon.2016.08.008.

[28] Y. Li, A. Kontsos, and I. Bartoli, "Automated Rust-Defect Detection of a Steel Bridge Using Aerial Multispectral Imagery," *Journal of Infrastructure Systems*, vol. 25, no. 2, Jun. 2019, doi: 10.1061/(asce)is.1943-555x.0000488.

[29] Y. Cai, "How Many Pixels Do We Need to See Things?," 2003.

[30] K. P. Sinaga and M. S. Yang, "Unsupervised K-means clustering algorithm," *IEEE Access*, vol. 8, pp. 80716–80727, 2020, doi: 10.1109/ACCESS.2020.2988796.

[31] "Manual for Bridge Element Inspection from IHS Markit," 2019.